Progress In Electromagnetics Research B, Vol. 23, 251–272, 2010

CIRCUITS AND ACTIVE ANTENNAS FOR ULTRA-WIDE BAND PULSE GENERATION AND TRANSMISSION

M. Kumar, A. Basu, and S. K. Koul

Centre for Applied Research in Electronics (CARE)
Indian Institute of Technology
Delhi, Hauz Khas, New Delhi-110016, India

Abstract—In this paper, the design and development of a novel active antenna including circuits for Ultra-wide band (UWB) pulse generation and transmission have been described. In this design a pulse with pulse-width approximately 150 ps and amplitude 500 mV (peak-to-peak) was generated using a single high electron mobility transistor (HEMT) as the active device (and an optional Schottky diode for enhanced performance), this being the simplest circuit for generating UWB pulses as far as we know. This circuit was integrated with a newly designed UWB planar microstrip-fed slot antenna, which is an active antenna in the sense that in addition to radiating the signal, it also acts as a filter, which tailors the spectrum of the transmitted pulse to a shape close to that recommended for UWB communications. We have also given a quantitative analysis, which explains the operation of the circuit.

1. INTRODUCTION

It is well known that the UWB communication system is a fast-emerging technology with unique attractive features promising major advances in wireless communications, networking, radar, imaging, and positioning systems.

UWB systems differ significantly from other wireless communication standards. In the best-known embodiment, this communicates using a series of narrow un-modulated pulses instead of using a high-frequency carrier. The pulse can be seen as a burst of RF energy where each pulse carries one symbol of information. UWB systems obviously

Received 21 May 2010, Accepted 16 July 2010, Scheduled 25 July 2010
Corresponding author: A. Basu (ananjan_b@yahoo.com).

cover a large spectrum, and unless properly handled, will interfere with existing users. In order to keep this interference to a minimum, the FCC-USA and other regulatory groups have specified spectral masks for different applications which show the allowed power output for specific frequencies [1, 2]. For the most commonly used UWB communication standard a large continuous bandwidth of 7.5 GHz is available between 3.1 GHz to 10.6 GHz at a maximum equivalent isotropic radiated power output of −41.3 dBm/MHz. Both the traditional pulse-based systems transmitting narrow pulses, which entirely or partially occupy the UWB bandwidth, and the systems based on orthogonal frequency-division multiplexing (OFDM) and similar techniques with a collection of narrowband carriers of at least 500 MHz can utilize the UWB spectrum under the FCC's rules.

One of the challenges for the implementation of UWB systems is the development of a suitable antenna. Many UWB antennas which are compact, planar and low-cost have been proposed [3–8]. Also 'active antenna' has been a growing area of research in recent years as microwave integrated circuit and monolithic microwave circuit technologies have become more mature allowing for higher levels of integration. The term 'active antenna' is too new to have a universally accepted definition; here it is used for a circuit which not only integrates the active microwave circuits and the radiating element on the same substrate, thereby reducing transition and transmission losses, but also utilizes the antenna for carrying out some circuit function (such as resonating or impedance-matching) apart from radiating or receiving radiation. Following this definition, it can be observed that while many active antennas have been demonstrated (for example [9]) none have been proposed for UWB systems. The circuit proposed in [6] uses the term 'active antenna' somewhat differently and does not describe any additional circuit functionality in the antenna. Here, the development of an antenna which carries out pulse-shaping in order to match the prescribed spectrum for UWB pulses will be described.

Numerous ultra-wideband, ultra-short-pulse transmitters have been developed — for example [10]. Most of these circuits are quite sophisticated, employing high-performance components and subsystems. The simplest circuit that has been described is in [11] and this also has used a step-recovery diode, which is a component incompatible with most MMIC/RFIC processes. In this paper, a new scheme for UWB pulse generation is proposed. To the best of our knowledge, this is the simplest circuit proposed for generating UWB pulses from a digital input, employing one FET, one optional diode and a few passive components. It can be implemented in MIC (employing distributed

approximations for L and C) or MMIC, and some extended form of CMOS-RF such as BiCMOS (if diode is required).

This paper is divided into four sections, the first one presenting an introduction and the scope of the paper. Section 2 presents a detailed account of UWB signal generation circuits starting from validation at low frequencies. A novel and simple method to generate UWB pulses using a BJT or a HEMT/MESFET is described, and a quantitative analysis to explain the principle of action is given. Experimental work to validate the simulated results at microwave frequencies (3–10 GHz) is presented in Section 3. Section 4 describes the UWB signal transmitter circuit incorporating an active antenna.

2. UWB SIGNAL GENERATION CIRCUIT

UWB signals have been usually generated using two techniques. One is to generate a narrow pulse using a differentiator-type circuit, and then modify the shape by filters [12] or an up-converter [13] to fit the FCC spectral mask. The other way is to generate a precise UWB pulse whose frequency spectrum satisfies the FCC regulation [14, 15]. High performance circuits following both approaches have been reported, but these have all been quite complex. In any case, the block diagram which describes the process is shown in Fig. 1. This is applicable to the circuits presented in this paper as well. The direct implementation of the first approach shown in Fig. 2 however leads to pulse-shapes are quite sensitive to rise and fall time. This is intuitively expected, and was verified using simple circuit simulation. More importantly, this approach produces pulses at both rising and falling edges of the input, and fairly complicated circuitry has to be used to eliminate one of them.

A new scheme is proposed for the generation of short pulse using a FET (use of a BJT is also possible) as an active device which overcomes these problems. These circuits are described next. We mention here that all simulations were done on Agilent ADS software.

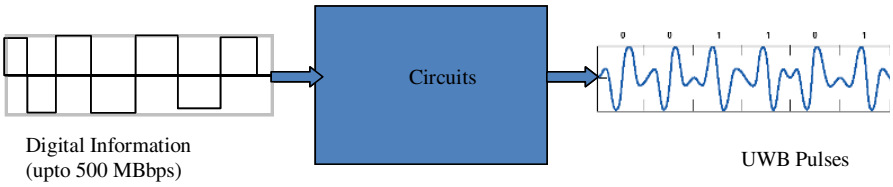

Figure 1. Generalized schematic for generation of UWB pulses.

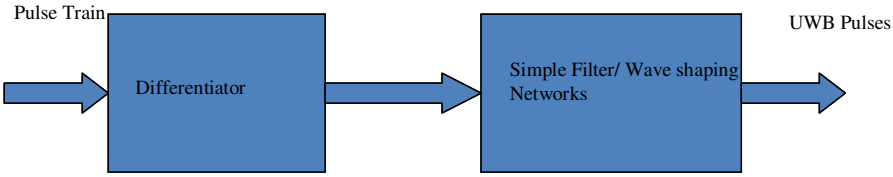

Figure 2. A simple implementation of UWB pulse generation scheme.

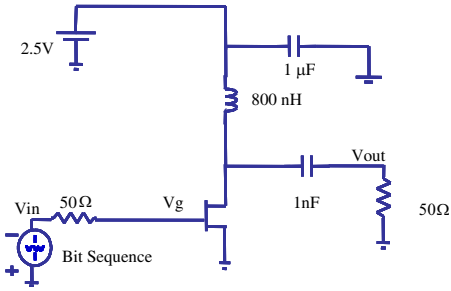

Figure 3. Basic short-pulse generation circuit at low frequency.

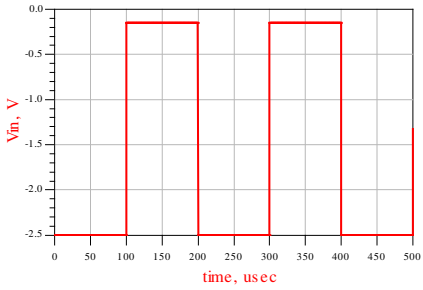

Figure 4. Input pulse train given to the circuit.

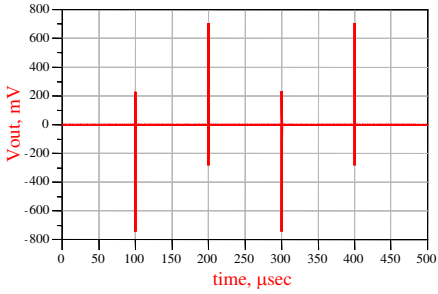

Figure 5. Output short pulses generated corresponding to the input pulse train.

2.1. Verification of Circuit at Low Frequency Using FET

In order to verify the principle of operation of the circuits, the HEMT-based circuit shown in Fig. 3 was tested at low frequencies. The L and C values connected to the drain were chosen to be 800 nH and 1 nF respectively. The input pulse train has following specification; $V_{low} = -2.5\,\text{V}$, $V_{high} = -0.15\,\text{V}$, pulse rate 5 kHz, as shown in Fig. 4. Rise and fall times were observed to be 100 ns. $V_{DC} = 2.5\,\text{V}$ was used for biasing the UWB circuit. Simulated plots of the generated

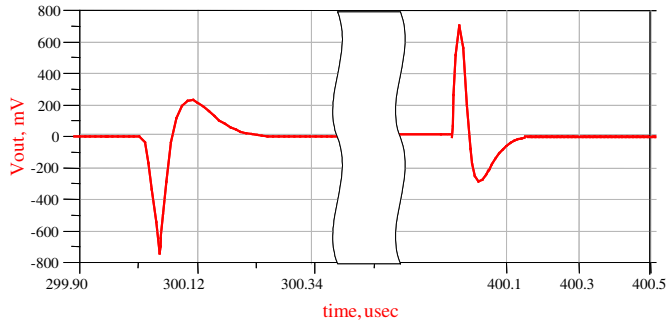

Figure 6. Zoomed view of output short pulse train generated from the basic short-pulse generation circuit.

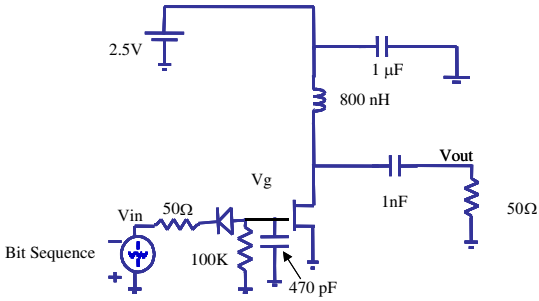

Figure 7. Modified short-pulse generation circuit at low frequency.

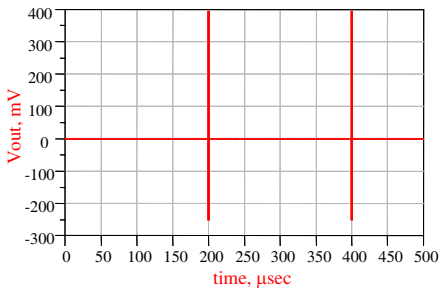

Figure 8. Output short pulse train generated from the modified circuit.

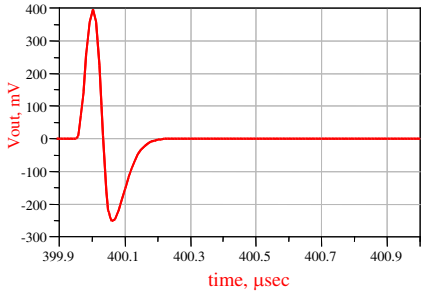

Figure 9. Zoomed view of output short pulse train generated from the modified circuit.

short pulses and their zoomed view are shown in the Fig. 5 and Fig. 6 respectively. In this case, we get output pulses corresponding to the rising as well as falling edges of input pulse train.

We have proposed a new scheme to get an output pulse only at

the falling edge of the input pulse train. The modified circuit is shown in Fig. 7. A packaged Schottky diode with wire leads, a resistance of 100 kΩ and capacitor of 470 pF were used in the input side of the transistor. The same input pulse that is shown in Fig. 4 is given to the circuit in the simulator and correspondingly we get the simulated output pulses that are shown in Fig. 8 with zoomed view in Fig. 9. The switching mechanism depends on the value of resistance R and capacitance C. The action of the diode is as follows: for the falling edge, the gate of the FET is rapidly pulled through the ON diode to the negative input voltage (−2.5 V). This causes an abrupt turn-off of the FET, thus abruptly diverting the drain current into the L-C at the output, which generates the UWB pulse. For the rising edge, the gate and the 470 pF capacitor have to discharge through the resistor R, the diode being OFF. This slows the turn-on of the FET, and the drain current rises gradually as shown in Fig. 10. This gradual turn-on leads to a negligibly weak output pulse generated by the L-C network at the rising edge of the input. This circuit was assembled on breadboard and tested on an oscilloscope. The input and output voltages were observed to have the expected waveforms, as shown in Fig. 11. The zoomed view shown in Fig. 12 confirms the simulations, the only difference being a distortion of the rising and falling edges of the input. This is not surprising, considering that the source is not an ideal voltage source. The operating principle of the circuit is however fully confirmed.

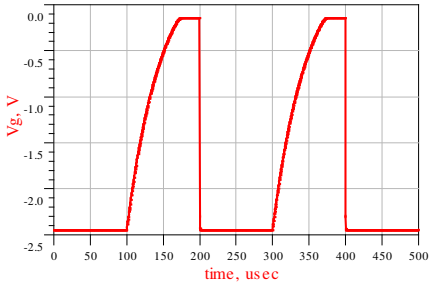

Figure 10. Gate voltage waveform for $R = 100\,\text{k}\Omega$ and $C = 470\,\text{pF}$.

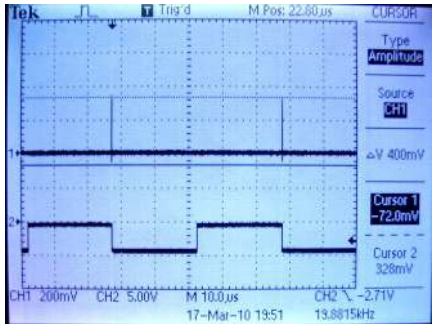

Figure 11. The measured input (lower trace) and output (upper trace) pulse trains from the modified circuit.

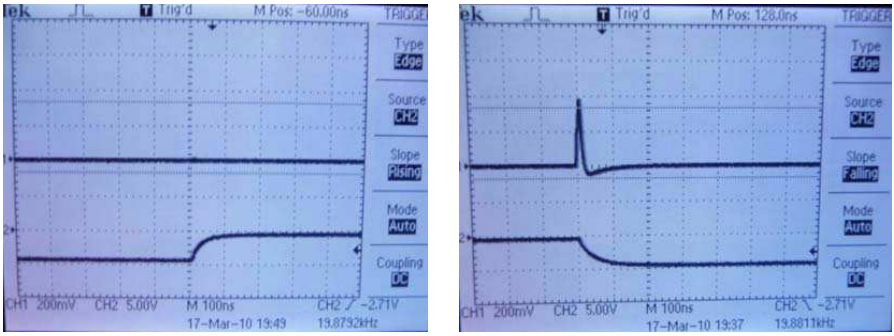

(a) (b)

Figure 12. Zoomed view of the measured output short pulse train generated by the modified circuit (a) corresponding to rising edge (b) and falling edge of input pulse train. The lower trace is the input signal in both (a) and (b).

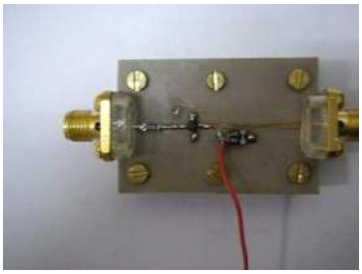

Figure 13. Practical circuit for generating UWB pulse.

2.2. Circuit for Generation of UWB Pulses for the 3.1–10.6 GHz Range

The fabricated circuit is shown in Fig. 13 and the output waveforms in Fig. 14. The details are given in [16]. While there is qualitative agreement between theory (Fig. 21) and experiment (Fig. 23), the differences are significant. These are caused by (a) the MIC capacitor (inter-digitated or parallel-plate type) being simulated as a simple capacitor and (b) the d.c. decoupling 1 μF capacitor being unable to remove the sub-nanosecond ripples from the voltage at the d.c input point. A practical solution to the second problem could not be found but the output waveform, while departing from the theory, is quite acceptable as a waveform to be used in a UWB system.

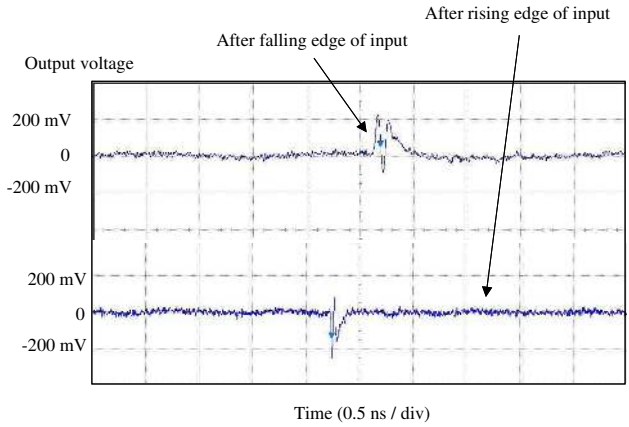

Figure 14. Measured output pulses from the circuit.

Before moving to a new circuit, which does not produce UWB pulses at rising as well as falling edges of the output, we next present an analysis of this circuit, which gives a better insight into its functioning.

2.3. Analysis of Circuit

A brief analysis of the circuit which better explains its action is presented. For a rising edge at the input, we assume that the device is initially in OFF state with some voltage across the capacitor, and at $t = 0$ it abruptly turns ON (with a low but finite R_{DS}). The resultant waveform at the output can then be calculated by standard transient circuit analysis, which also predicts the final current in the inductor. This is used as an initial condition for analyzing the turn-OFF. When the device is turned OFF by the input going low, the output waveform can be calculated by analyzing the *L*-*C*-*R* circuit, ignoring R_{DS} and C_{DS}.

2.3.1. FET in Turn-on State

When transistor is working in the turn-on state, the equivalent circuit is shown in Fig. 15. The on-state resistance (R_{DS}) of the FET is calculated using the data sheet provided by manufacture that is shown in the Fig. 16, and came out to be $10\,\Omega$.

In the circuit shown in Fig. 15 the load resistance R_L is $50\,\Omega$. Initially capacitor C is charged upto the voltage V_{DS} when the transistor remains in OFF condition and current flowing through the inductor is zero. So $I(L) = 0$ and $V(C) = V_{DC}$ at $t = 0^-$. The relevant

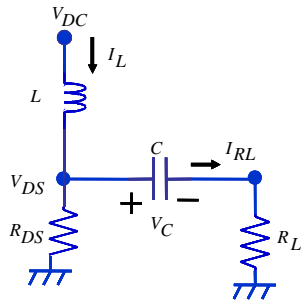

Figure 15. The equivalent circuit for FET turn-on.

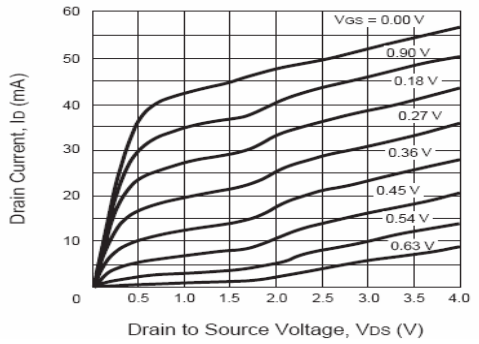

Figure 16. Drain current versus drain to source voltage characteristic of FET.

equations are:

$$I_{R_L} = \frac{V_{DS} - V_C}{R_L} \tag{1}$$

$$V_{DS} = V_{DC} - L\frac{dI_L}{dt} \tag{2}$$

$$I_L = \frac{V_{DS}}{R_{DS}} + I_{R_L} \tag{3}$$

$$I_{R_L} = C\frac{dV_C}{dt} \tag{4}$$

By simplifying the Equations (1), (2) and (4),

$$I_L = \frac{V_{DC} - L\frac{dI_L}{dt}}{R_{DS}} + C\frac{dV_C}{dt} \tag{5}$$

By simplifying (1), (2), (3), and (4),

$$C\frac{dV_C}{dt}R_L = V_{DC} - L\frac{dI_L}{dt} - V_C(t) \tag{6}$$

Laplace transformation is utilizing to solve the Equations (5) and (6).

$$CR_L(sV_C - V_{DC}) = \frac{V_{DC}}{s} - L(sI_L - 0) - V_C \tag{7}$$

$$I_L = \frac{V_{DC}/s - (sLI_L - 0)}{R_{DS}} + C(sV_C - V_{DC}) \tag{8}$$

Using Equations (7) and (8)

$$I_L = \frac{(V_{DC}CR_L/(LCR_L + R_{DS}CL))\left(s + \frac{1}{CR_L}\right)}{s\left(s^2 + s\frac{CR_LR_{DS}+L}{LCR_L+R_{DS}CL} + \frac{R_{DS}}{LCR_L+R_{DS}CL}\right)} \tag{9}$$

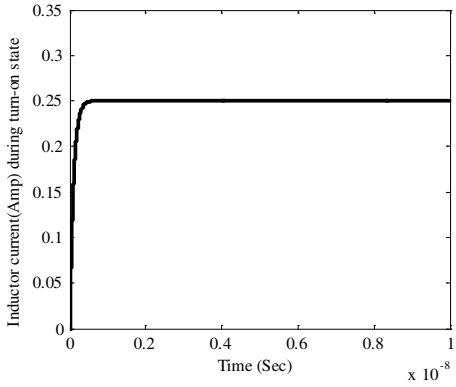

Figure 17. The transient response of current is flowing in the inductor during transistor turn-on.

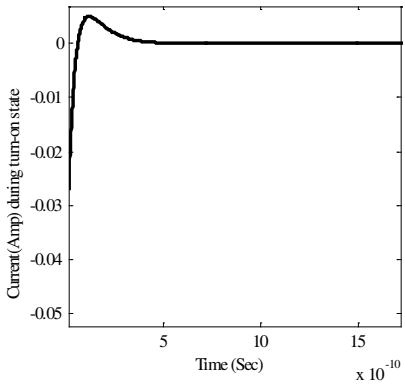

Figure 18. The transient response of output current flowing in the load resistance during transistor turn-on, showing the discontinuous dip at $t = 0$.

By inverting this in the usual way, and using the equation: $I_{R_L} = I_L - \frac{V_{DC} - L\frac{dI_L}{dt}}{R_{DS}}$, the output current flowing in load can be calculated.

The transient response graphs are calculated by putting the values; $V_{DC} = 2.5\,\text{V}$, $L = 1\,\text{nH}$, $C = 0.6\,\text{pF}$, $R_{DS} = 10\,\Omega$, and $R_L = 50\,\Omega$. The current flowing in the inductor during transistor turn-on is shown in Fig. 17 and the load current response is shown in the Fig. 18.

2.3.2. FET in Turn-off State

When transistor is working in the turn-off state, the equivalent circuit is shown in Fig. 19(a). The value of capacitance (C_{DS}) of the FET is 0.12 pF and it can be neglected for simplification.

Let loop current be i flowing in the circuit. In the time domain application of KVL to the circuit gives:

$$L\frac{di}{dt} + \left[\frac{1}{C}\left(\int_0^t idt\right) + V_C(t=0)\right] + R_L i = V_{DC} \tag{10}$$

$$\text{For} \quad t = 0^+, \quad L\left.\frac{di}{dt}\right|_{t=0^+} + \frac{1}{C}V_C(t=0^+) + R_L i(t=0^+) = V_{DC} \tag{11}$$

We know that the initial current $i(t = 0^+)$ present in the inductor due to turn-on condition of the transistor. i.e., $i(t = 0^+) = I_0 = 0.25\,\text{A}$ (the first initial condition) and $V_C(t = 0) = V_{DC}$.

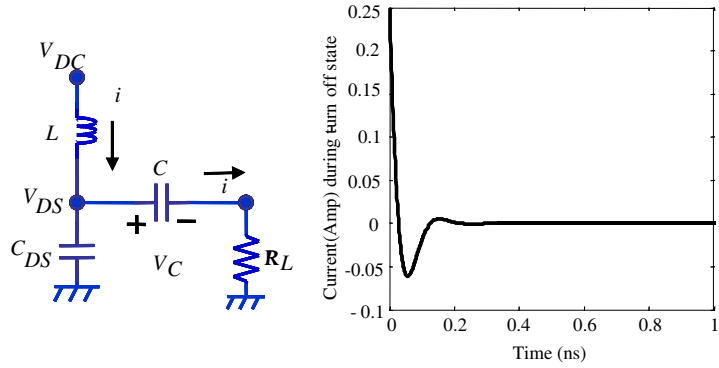

(a) (b)

Figure 19. (a) The equivalent circuit in the turn-off condition of FET. (b) The transient response of current (i).

$L\left.\frac{di}{dt}\right|_{t=0^+} + V_{DC} + R_L I_0 = V_{DC}$, leading to: $\left.\frac{di}{dt}\right|_{t=0^+} = \frac{-R_L I_0}{L}$, the second initial condition.

Put the value of $I_0 = 0.25\,\text{A}$, $R_L = 50\,\Omega$, and $L = 1\,\text{nH}$.

$$\left.\frac{di}{dt}\right|_{t=0^+} = -1.25 \times 10^{10} \tag{12}$$

By differentiating (10),

$$\frac{d^2 i}{dt^2} + \frac{R_L}{L}\frac{di}{dt} + \frac{1}{LC} i = 0 \tag{13}$$

The solution of this is known to be $i = C_1 e^{P_1 t} + C_2 e^{p_2 t}$, where

$$p_1, p_2 = \frac{-R_L \Big/ L \pm \sqrt{(R_L/L)^2 - 4/LC}}{2}$$

By putting the values of the parameters $L = 1\,\text{nH}$, $C = 0.6\,\text{pF}$, and $R_L = 50\,\Omega$,

$p_1 = \alpha + j\beta = -2.5\times10^{10} + j3.3\times10^{10}$, $\quad p_2 = \alpha - j\beta = -2.5\times10^{10} - j3.23\times10^{10}$

This can also be written as:

$$i = e^{\alpha t}\left(A\cos\beta t + jB\sin\beta t\right) \tag{14}$$

Using the initial conditions, we get the final result:

$$i(t) = e^{-2.5\times10^{10} t}\left\{0.25\cos(3.23\times10^{10} t) - 0.1934\sin(3.23\times10^{10} t)\right\} \tag{15}$$

The transient response graph of output current, when transistor abruptly turns off is plotted is shown in Fig. 19(b).

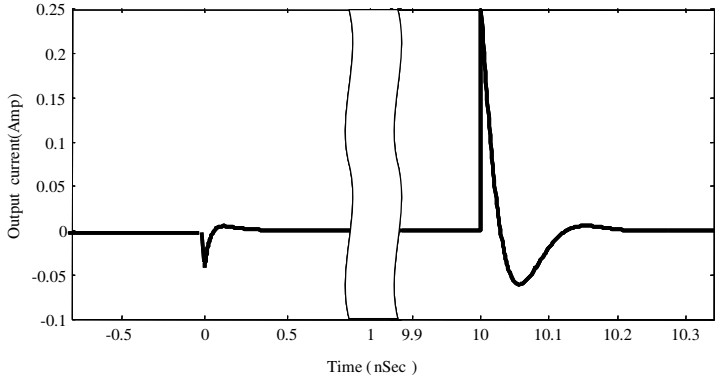

Figure 20. The complete transient response of output current in the UWB generation circuit.

Combining the turn-ON and turn-OFF, with an input pulse-width of 10 ns, we get the final load current waveform in Fig. 20, which may be compared to the simulated result in Fig. 6 or the measured results in Fig. 12(b) (only the pulse at the falling edge) and Fig. 14. Note that the output pulse during turn-on is quite small, but may still pose problems if ignored — leading to the modified circuit where it is practically eliminated.

3. IMPROVED CIRCUIT FOR GENERATION OF UWB PULSES FOR 3.1–10.6 GHz RANGE

To obtain pulses only at one edge (in this case, the falling edge) of the input, we use the circuit from Fig. 7, with modified component values as shown in Fig. 21. In this scheme, we have connected a diode and a resistance R at the input. Only one pulse was achieved in the output corresponding to the falling edge of the input pulse as has already been described in [17], and further details are omitted. A number of microstrip line sections are shown in Fig. 21 — except the one joining the inductor and the capacitor, these are not required, and are essential only for laying out a practical circuit. The small 10 nF (for high frequency spurious removal) and the physically larger 1 μF capacitors are essential in order to stabilize the DC supply to the circuit. Distortion of the supply waveform was found to be the principal contributor to distortions in the output pulse-shape. The generated pulse-shapes when one or both of the supply stabilization capacitors is removed, are shown in Fig. 22. All these issues will automatically get resolved in an MMIC/RFIC realization.

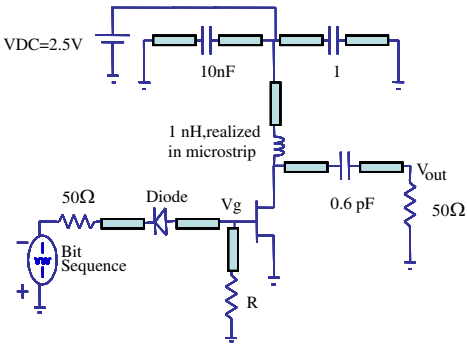

(a)

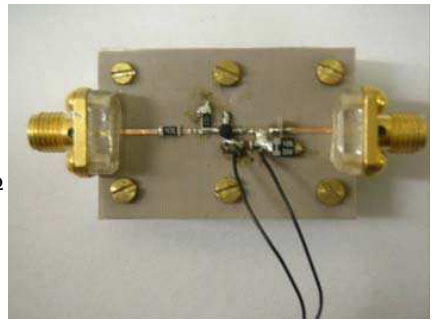

(b)

Figure 21. (a) New circuit for generation of UWB pulses. (b) The fabricated circuit.

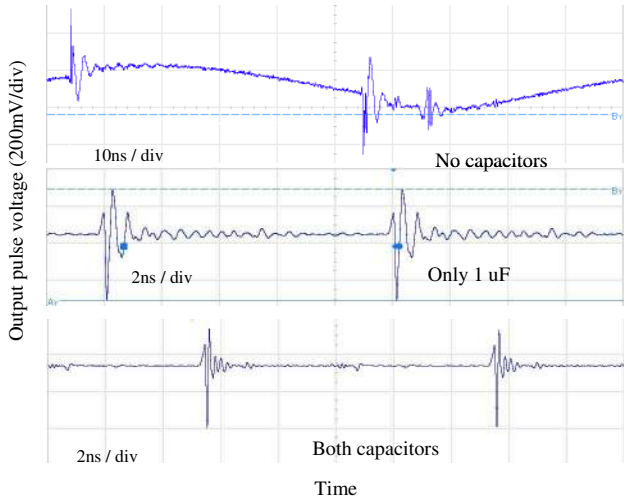

Figure 22. Effect of supply stabilization capacitors on output pulse shape.

The fabrication and testing of this circuit has been described in detail in [17], and in Fig. 23(a) we show the best pulse-shape that we have been able to obtain till now. Fig. 23(b) shows a comparison with the pulse-shape obtained by simulating the circuit of Fig. 21. It is seen that the main pulse occupies ~ 0.5 ns in time domain and roughly the prescribed bandwidth of 3–10 GHz in frequency domain. Even counting the small ringing in the pulse, the duration is < 1.5 ns, which is more than satisfactory for data transmission at 500 Mbps, as will be seen in Fig. 29.

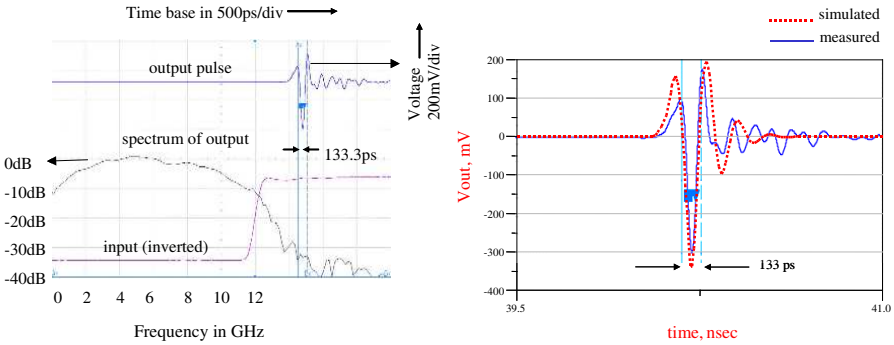

Figure 23. (a) Input pulse (inverted), output pulse, and spectrum of output (normalized to peak), (b) the output pulse-shape compared to simulation.

4. UWB ACTIVE ANTENNA

Numerous antennas for UWB applications have been reported, for example [18–22]. We report here a UWB 'active antenna', where the term is used in the sense explained in Section 1.

In [6], it is seen that the measured transmission coefficient from one antenna to another experiences large variation for higher operating frequencies. To reduce this variation in the range of 3.1 to 10.6 GHz, and keep the transmission very low outside this band, we have proposed slot antennas that give almost flat response in this range. The antennas thus implement spectrum-shaping, in addition to radiating and receiving radiation. While a kind of slot antenna has been proposed for UWB [22], it is a much more complicated structure — we have used the traditional microstrip-fed narrow rectangular ground-plane slot as shown in Fig. 24(a).

The slot antennas used are fairly conventional, as shown in Fig. 24. The length L_m of the open-circuited microstrip stub is approximately a quarter-wave long so that an effective short circuit is realized at the outer edge of the slot as shown in Fig. 24(a). Fig. 24(b) shows the dimensions of a circular monopole (representative of numerous similar antennas reported recently, such as [18]), which we have also investigated in order to compare our results to existing antennas. Since we could not find a reference for a circular monopole with all dimensions specified, the dimensions in Fig. 24(b) were obtained after detailed simulations for our own structure. However, a study of these antennas shows that qualitatively their properties are quite similar, and the conclusions below apply to most antennas of this class.

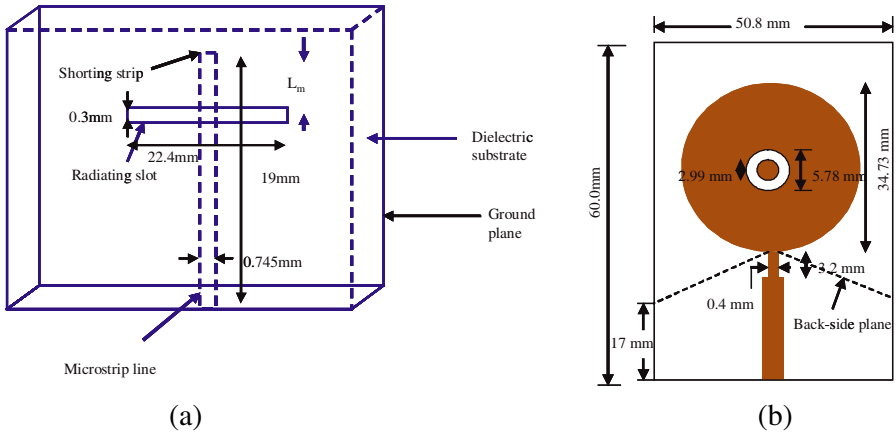

Figure 24. (a) Slot antenna dimensions, and (b) circular monopole dimensions.

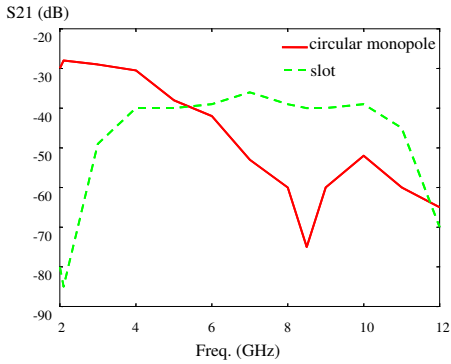

Figure 25. Measured $|S_{21}|$ for printed monopole and slot antennas. Separation between identical back-to-back antennas is 15 cm for both cases.

The return loss of the slot antenna (Fig. 26(b)) is not good at the lower frequencies. The emphasis here is on obtaining a constant insertion loss from transmitting antenna to receiving, and not on improving return loss. The benefit realized at the expense of sub-optimal return loss is shown in Fig. 25.

Measured insertion loss $|S_{21}|$ of 2 antennas separated by 15 cm is shown in Fig. 25. Here microstrip feed of the transmitter is port 1 and microstrip feed of the receiver is port 2. The plots are shown for two cases — a conventional circular monopole (representative of a

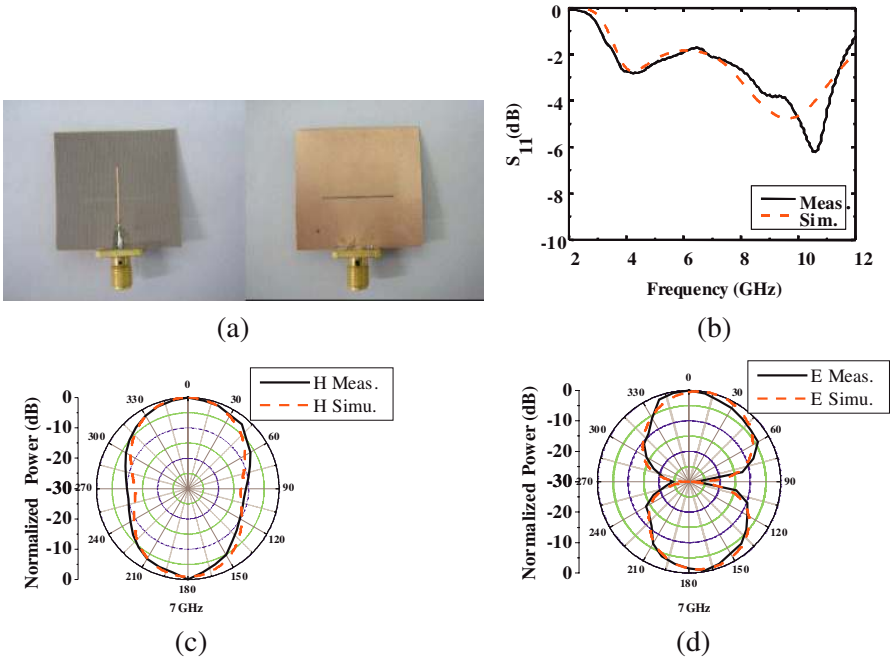

Figure 26. (a) The fabricated slot antenna structure, (b) its return loss, (c) H-plane (perpendicular to feed-line) radiation pattern at 7 GHz, (d) E-plane (perpendicular to slot) radiation pattern at 7 GHz. 0° is perpendicular to the substrate from the feed side.

large class of UWB antennas proposed in recent times), and our newly-proposed slot antenna. It is clear that our antenna uses the 3–10 GHz band much more efficiently than the printed monopole.

The simulated E-plane and H-plane radiation pattern are similar to conventional slot antenna. Detailed study of these antennas (as regards radiation pattern and insertion loss) has been carried out and these results will be shortly reported separately.

These fabricated slot antenna is shown in the Fig. 26(a), its return loss (measured with microstrip TRL calibration and simulated) in Fig. 26(b), its H-plane radiation pattern (measured and simulated) at a mid-band frequency of 7 GHz in Fig. 26(c), and E-plane radiation pattern (measured and simulated) in Fig. 26(d). The agreement between measured and simulated data is fairly good — the only discrepancy which we cannot explain yet is the 0.5 GHz shift in the frequency of best return loss. The most probable explanation is change in dielectric constant from the manufacturer-specified 2.2 at 10 MHz

to around 2.0 at 10 GHz, but this is unconfirmed. These plots are similar to those reported in the literature for many UWB antennas, but very importantly, these are almost the same throughout the 3–10 GHz range. The gain at 7 GHz was measured to be 3 dB (using comparison with a standard gain horn) while the simulated directivity was 6 dB, leading to an efficiency of 50% which is reasonable. Simulation of gain was not attempted due to uncertainty in microstrip to soldered connector transition, which we have found to be significant, but not predicted well in simulations. The antennas were also tested on a vector network analyzer. Measured magnitude and group delay of S_{21} are shown in Fig. 27.

Finally one slot antenna was integrated with the pulse generating circuit, and another was used as the receiver. A photo of the transmitter circuit and a plot of the pulse shapes received from this are shown in Fig. 28. Fig. 29 shows that communication upto 500 Mbps is quite possible using such pulses, although issues of bit-error-rate with (possibly quite substantial) noise and interference and receiver design are not addressed here. The spectrum of these pulses is shown in Fig. 30. A 10 dB attenuator has been used between the circuit and the antenna to reduce out-of-band reflections from the antenna. For comparison, the changed spectrum when a simple printed circular monopole UWB antenna is used is shown in Fig. 31. It is observed that there is significant power transmitted in the 2–3 GHz region which is not acceptable for UWB communication. For completeness, we mention here that by spectrum, we mean the Fourier transform of

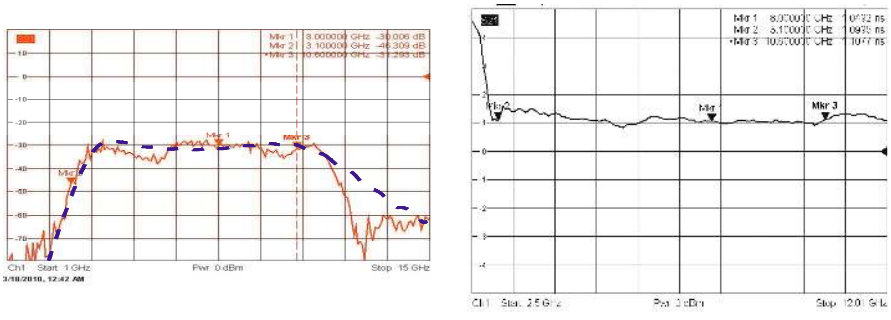

(a) (b)

Figure 27. (a) Measured $|S_{21}|$ (solid) with simulated $|S_{21}|$ (dashed), for inter-antenna spacing 15 cm and (b) group delay of transmitting-receiving antenna pair.

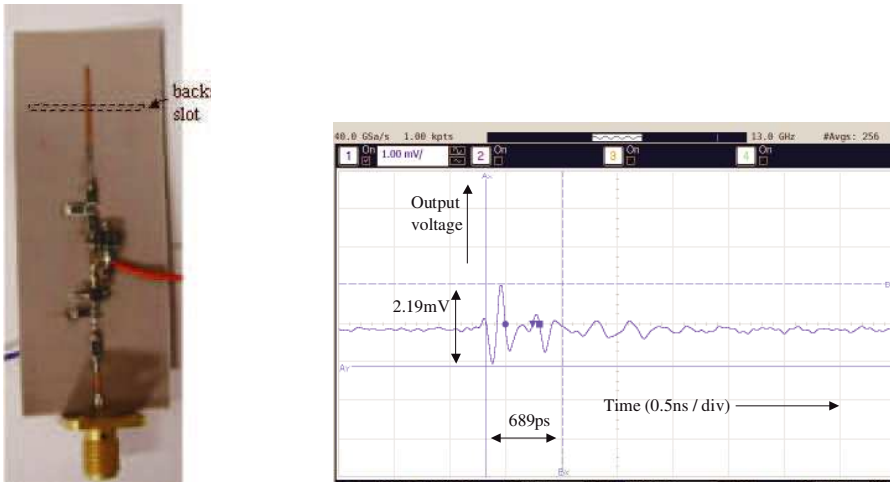

Figure 28. (a) Complete transmitter circuit with active antenna, (b) received UWB pulse (close approximation to the 'Gaussian doublet').

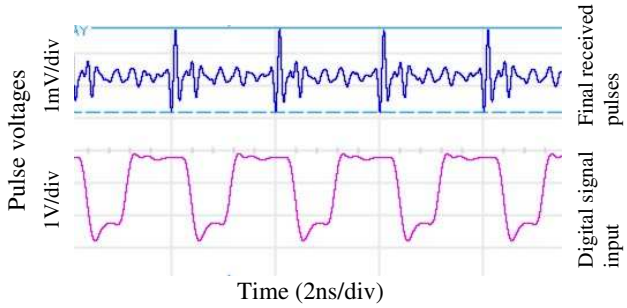

Figure 29. Communication at 500 Mbps: The digital input (lower trace), and UWB pulses after passing through the transmitting to receiving antenna channel (upper trace).

the waveform, defined in this case by the following equation:

$$V(f) = \frac{1}{T}\int_0^T v(t)e^{-j(2\pi f)t}dt \tag{16}$$

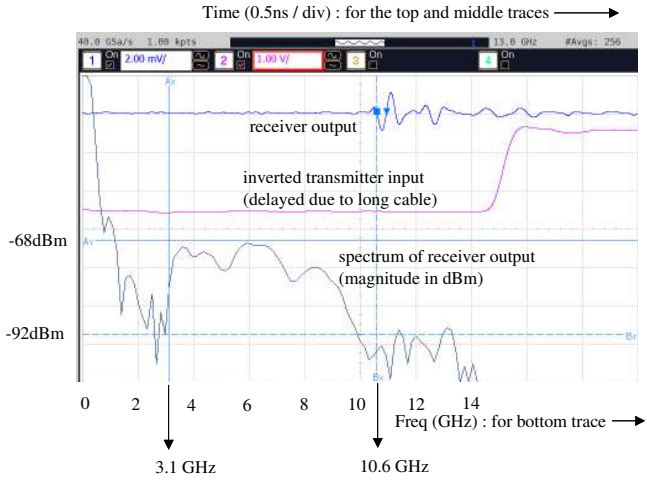

Figure 30. Spectrum of received pulse.

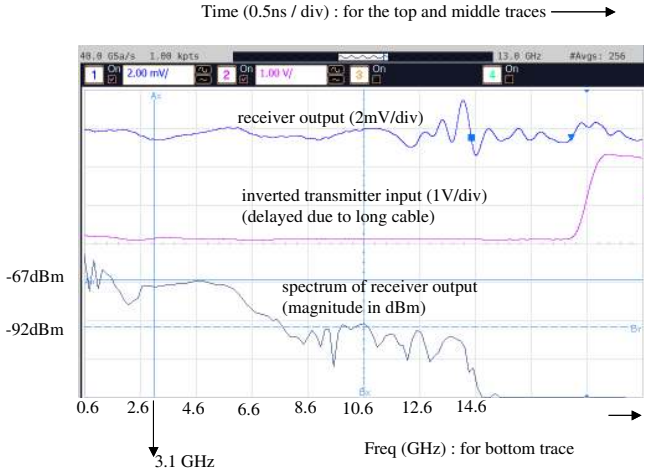

Figure 31. Received pulse waveform and spectrum using conventional UWB antenna.

Its magnitude is plotted in dBm using the following expression:

$$V_{\mathrm{dBm}}(f) = 10\log\left(\frac{2|V(f)|^2/50}{0.001}\right), \tag{17}$$

the factor of 2 being used to account for the power in negative frequencies.

For an oscilloscope sampling rate of N samples/sec, and a data set of P points, T obviously comes out to (P/N) sec. N and P are displayed with the plots above.

5. CONCLUSION

A novel UWB pulse generating circuit and an active UWB antenna have been developed. This circuit is the simplest known for generating UWB pulses, is low cost and is compatible with MMIC (and probably RF-CMOS with simple modifications), which is important for practical UWB systems. In future UWB communication systems which include antenna arrays, multiple transmitters and appropriate receiver will be developed.

ACKNOWLEDGMENT

The authors wish to acknowledge the assistance of Agilent Technologies for providing the high-speed oscilloscope and for a donation of ADS software.

REFERENCES

1. Ghavami, M., L. B. Michael, and R. Kohno, *Ultra Wideband Signals and Systems in Communication Engineering*, John Wiley & Sons, Ltd, England, 2004.
2. Federal Communications Commission, "First report and order," Feb. 14, 2002.
3. Ammann, M. J. and Z. N. Chen, "Wideband monopole antenna for multi-band wireless system," *IEEE Antenna Propag. Mag.*, Vol. 45, No. 2, 146–150, 2003.
4. Kharakhili, F. G., M. Fardis, G. Dadashzadeh, A. K. A. Ahmadi, and N. Hojjat, "Circular slot with a novel circular microstrip open ended microstrip feed for UWB applications," *Progress In Electromagnetics Research*, Vol. 68, 161–167, 2007.
5. Chen, H.-D. and H.-T. Chen, "A CPW-fed dual-frequency monopole antenna," *IEEE Trans. Antenna Propagation*, Vol. 52, 978–982, Apr. 2004.
6. Antonino, D. E., F. M. Cabedo, B. Ferrando, and A. J. Villa, "Active UWB antenna with tunable band-notch behaviour," *Electronics Letters*, Vol. 43, No. 18, Aug. 31, 2007.

7. Lin, C.-C. and H.-R. Chuang, "A 3–12 GHz UWB planar triangular monopole antenna with ridged ground-plane," *Progress In Electromagnetics Research*, Vol. 83, 307–321, 2008.
8. Chen, Z. N., *Antenna for Portable Devices*, John Wiley & Sons, Ltd, England, 2007.
9. Kumar, M., A. Basu, S. K. Koul, and B. Bhat, "Active suspended microstrip patch antenna," *PIERS Proceedings*, 180, Osaka, Japan, Jul. 18–22, 2001.
10. Ma, T.-G., C.-J. Wu, and C.-F. Chou, "An impulse-radio-based ultrawideband RF front-end module with a new multilayered microwave sampler," *Progress In Electromagnetics Research*, Vol. 86, 1–18, 2008.
11. Jeong, S. L. and C. Nguyen, "Novel low-cost ultra-wideband, ultra-short-pulse transmitter with MESFET impulse-shaping circuitry for reduced distortion and improved pulse repetition rate," *IEEE Microwave and Wireless Components Letters*, Vol. 11, No. 5, 208–210, May 2001.
12. Saha, P. K., N. Sasaki, and T. Kikkawa, "A CMOS UWB transmitter for intra/inter-chip wireless communication," *International Symposium on Spread Spectrum Techniques and Applications 2004*, 962–966, Sep. 2004.
13. Ryckaert, J., et al., "Ultra-wide-band transmitter for low power wireless body area networks: Design and evaluation," *IEEE Transactions on Circuits and Systems*, Vol. 52, 2515–2525, Dec. 2005.
14. Kim, H. and Y. Joo, "Fifth-derivative Gaussian pulse generator for UWB system," *IEEE Radio Frequency Integrated Circuits Symposium*, 671–674, Jun. 2005.
15. Norimatsu, T., et al., "A novel UWB impulse-radio transmitter with all-digitally-controlled pulse generator," *European Solid-state Circuits Conference 2005*, 267–270, 2005.
16. Kumar, M., A. Basu, and S. K. Koul, "A novel scheme for generating and transmitting UWB signals," *Proceedings of 2009 IEEE International Conference on Antennas, Propagation and Systems (INAS 2009)*, Johor Bahru, Malaysia, Dec. 3–5, 2009.
17. Kumar, M., A. Basu, and S. K. Koul, "Electromagnetic short pulse generation techniques," *The 2010 International Symposium on Electromagnetic Theory (EMTS 2010)*, Berlin, Germany, Aug. 16–19, 2010.
18. Liang, J., L. Guo, C. C. Chiau, X. Chen, and C. G. Parini, "Study of CPW-fed circular disc monopole antenna for ultra wideband

applications," *IEE Proceedings on Microwaves, Antennas and Propagation, IET Journals*, 520–526, 2005.

19. Chen, D. and C. H. Cheng, "A novel compact ultra-wideband (UWB) wide slot antenna with via holes," *Progress In Electromagnetics Research*, Vol. 94, 343–349, 2009.
20. Sadat, S., M. Houshmand, and M. Roshandel, "Design of a microstrip square-ring slot antenna filled by an H-shape slot for UWB applications," *Progress In Electromagnetics Research*, Vol. 70, 191–198, 2007.
21. Zaker, R., C. Ghobadi, and J. Nourinia, "A modified microstrip-FED two-step tapered monopole antenna for UWB and WLAN applications," *Progress In Electromagnetics Research*, Vol. 77, 137–148, 2007.
22. Siahcheshm, A., S. Sadat, C. H. Ghobadi, and J. Nourinia, "Design of a microstrip slot antenna filled by an isosceles triangle for UWB applications," *Journal of Electromagnetic Waves and Applications*, Vol. 22, No. 1, 111–118, 2008.